HHS Public Access

Author manuscript

Cell Rep. Author manuscript; available in PMC 2021 April 15.

Published in final edited form as:

Cell Rep. 2020 June 09; 31(10): 107730. doi:10.1016/j.celrep.2020.107730.

Mature Retina Compensates Functionally for Partial Loss of Rod Photoreceptors

Rachel A. Care[1], **Ivan A. Anastassov**[2], **David B. Kastner**[3], **Yien-Ming Kuo**[4], **Luca Della Santina**[4,*], **Felice A. Dunn**[4,5,*]

[1]Graduate Program in Neuroscience, University of California, San Francisco, San Francisco, CA 94158, USA

[2]Department of Biology, San Francisco State University, San Francisco, CA 94132, USA

[3]Department of Psychiatry, University of California, San Francisco, San Francisco, CA 94143, USA

[4]Department of Ophthalmology, University of California, San Francisco, San Francisco, CA 94143, USA

[5]Lead Contact

SUMMARY

Loss of primary neuronal inputs inevitably strikes every neural circuit. The deafferented circuit could propagate, amplify, or mitigate input loss, thus affecting the circuit's output. How the deafferented circuit contributes to the effect on the output is poorly understood because of lack of control over loss of and access to circuit elements. Here, we control the timing and degree of rod photoreceptor ablation in mature mouse retina and uncover compensation. Following loss of half of the rods, rod bipolar cells mitigate the loss by preserving voltage output. Such mitigation allows partial recovery of ganglion cell responses. We conclude that rod death is compensated for in the circuit because ganglion cell responses to stimulation of half of the rods in an unperturbed circuit are weaker than responses after death of half of the rods. The dominant mechanism of such compensation includes homeostatic regulation of inhibition to balance the loss of excitation.

Graphical Abstract

*Correspondence: luca.dellasantina@ucsf.edu (L.D.S.), felice.dunn@ucsf.edu (F.A.D.).

AUTHOR CONTRIBUTIONS

Conceptualization, R.A.C., I.A.A., D.B.K., and F.A.D.; Methodology, R.A.C., I.A.A., L.D.S., Y.-M.K., and F.A.D.; Software, R.A.C., L.D.S., D.B.K., and F.A.D.; Validation, F.A.D.; Formal Analysis, R.A.C., I.A.A., L.D.S., and F.A.D.; Investigation, R.A.C., I.A.A, L.D.S., and F.A.D.; Resources, Y.-M.K.; Data Curation, R.A.C., L.D.S., and F.A.D.; Writing – Original Draft, R.A.C. and F.A.D.; Writing – Review & Editing, R.A.C., I.A.A., L.D.S., and F.A.D.; Visualization, R.A.C. and F.A.D.; Supervision, F.A.D.; Project Administration, R.A.C. and F.A.D.; Funding Acquisition, R.A.C. and F.A.D.

SUPPLEMENTAL INFORMATION

Supplemental Information can be found online at https://doi.org/10.1016/j.celrep.2020.107730.

DECLARATION OF INTERESTS

The authors declare no competing interests.

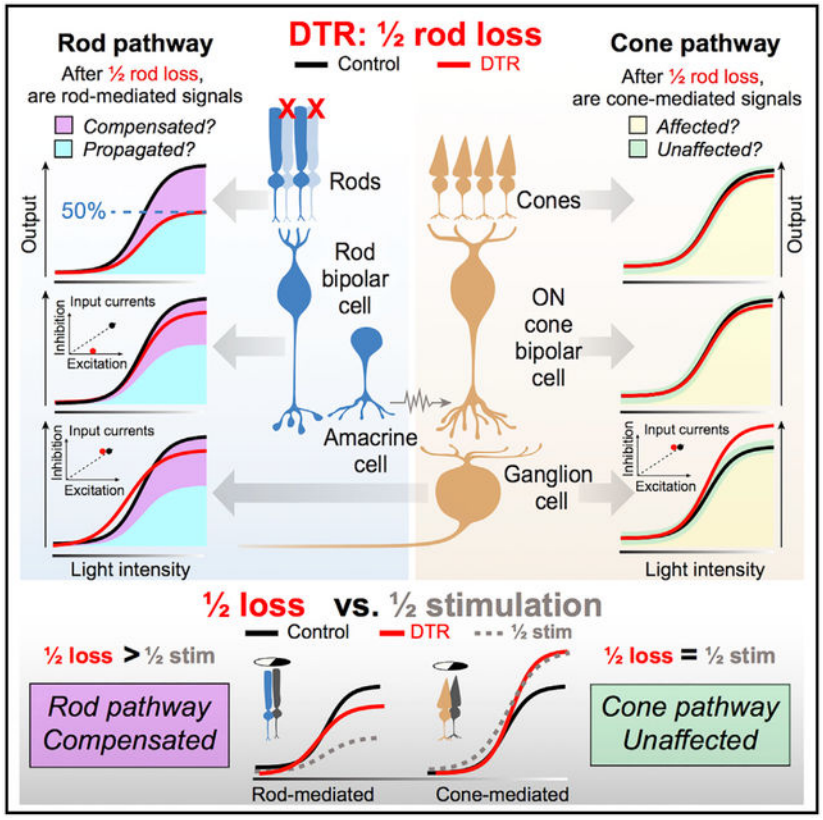

In Brief

Care et al. ablate half of the rods in mature mouse retina and find that primary neuron loss is functionally compensated for by balanced inhibition and excitation at the secondary neuron. Changes in cone-mediated, but not rod-mediated, output neuron spikes are recapitulated by half stimulation, demonstrating independent regulation of pathways.

INTRODUCTION

Degenerative diseases, injury, and normal aging can cause the death of primary neurons. Understanding the changes that happen in the resulting deafferented neural circuits is critical for diagnostic and therapeutic efforts to preserve and rescue function. Input loss may be propagated through a deafferented circuit, resulting in a decrease in output proportional to the decrease in input. Input loss may also be exacerbated, for example through degeneration of initially unaffected neurons, leading to a decrease in output more severe than the decrease in input. Alternatively, input loss may be compensated for within a deafferented circuit, resulting in a full or partial recovery of the output signal. To differentiate between these possibilities, we must investigate a circuit with known, controllable inputs and highly stereotypic outputs. To pinpoint the origin of compensation within a deafferented circuit, we use the retina, a system with accessible and identifiable neurons.

Previous studies of input loss in mature retina have performed focal lesions in primary sensory neurons and have demonstrated that the ganglion cell's spatial receptive fields fill in

the resulting scotoma (Sher et al., 2013; Beier et al., 2017). Our study of partial cone loss further demonstrated that the ganglion cell's receptive field expanded its inhibitory surround yet maintained center-surround organization (Care et al., 2019)—a fundamental function of ganglion cell processing (Kuffler, 1953; Barlow, 1953; Atick and Redlich, 1990). A recent study using the same partial cone ablation suggested that specific bipolar cell types can regain photoreceptor contacts (Shen et al., 2020). These findings suggest the mature retina may compensate for input loss, but the mechanisms and extent of such compensation remain unclear.

Here, in mature retina, we induce death in half of rods, which in the mouse comprise half of the entire population of primary sensory neurons, and measure function throughout the partially deafferented circuit to identify potential sites of compensation. We record the output of the retina from alpha ON sustained ganglion cells ($A_{ON\text{-}S}$ GCs) (Margolis and Detwiler, 2007; van Wyk et al., 2009; Krieger et al., 2017). These cells are arguably the most well-characterized and sensitive ganglion cells in mouse retina and would therefore reflect changes in the circuit at low light levels dominated by rod input (Murphy and Rieke, 2006; Margolis and Detwiler, 2007; van Wyk et al., 2009; Krieger et al., 2017). Light responses initiated by rods proceed via synaptic transmission to rod bipolar cells (RBCs) and then to AII amacrine cells, which are electrically coupled to ON cone bipolar cells (CBCs) (Figure 1A). The rod and cone pathways converge in the ON cone bipolar cells' axon terminals, which synapse onto ganglion cell dendrites. Similarly, we record from alpha OFF transient ganglion cells ($A_{OFF\text{-}T}$ GCs), which rely on a pathway that diverges at the AII amacrine cell-to-OFF cone bipolar cell synapse, to generalize our results. We use these well-defined pathways to examine the consequences of partial rod death on the deafferented circuit.

We show that by the retinal output, the ganglion cells have largely compensated for half rod loss in their rod-mediated spikes and excitatory input currents. We localize compensation at the level of the rod bipolar cell, where reduced excitatory input currents are compensated for by reduced inhibitory currents resulting in recovered voltage outputs. Intriguingly, in the same ganglion cells that show recovered rod-mediated light responses, cone-mediated light responses are enhanced. These changes in cone-mediated, but not rod-mediated, responses are recapitulated by half stimulation of control retina, allowing us to differentiate reduced rod input from subsequent compensatory changes within the partially deafferented circuit.

RESULTS

Selective Ablation of Half of Rod Photoreceptors in Mature Mouse Retina

To induce partial rod loss, we injected diphtheria toxin (DT) into mice expressing the diphtheria toxin receptor (DTR) under the rhodopsin promoter at postnatal day 30 (Rho-DTR) (Figure 1A). In this system, half of the rods are ablated upon examination 1 month after DT injection (Figure 1B; STAR Methods). Control mice, either DTR-positive or -negative, were injected with saline. Rod death was confirmed in cross-sections of retina by quantifying the rows of somata present in the outer nuclear layer (ONL), which is composed of 97.2% rods (Jeon et al., 1998; Figure 1C). Two injections of DT consistently reduced the rod population by 50%–60% (Figure 1D, ONL) (Control, 10.3 ± 0.44, n = 10; DTR, 4.1 ± 0.22 rows of somas, n = 7; median ± interquartile range [IQR], p = 4.57e-05, rank sum). To

examine off-target effects, we quantified the rows of somata present in the inner nuclear layer (INL), which is composed of bipolar and amacrine cell somas, and found no change after rod death (Figure 1D, INL) (control, 4.47 ± 0.27, n = 10; DTR, 4.33 ± 0.20 rows of somas, n = 7; median ± IQR, p = 0.371, rank sum). Quantification of cones, horizontal cells, rod bipolar cells, starburst amacrine cells, ganglion cells, and microglia immunostained in flat mount retina revealed no reduction (Figure S1; Table S1). Furthermore, when the Rho-DTR mouse line was crossed to a fluorescent reporter mouse line, fluorescence was confined to rods (Figure S2). With this system that selectively ablates rods, we aimed to understand how the mature retina reacts to input loss. The retinal reaction to input loss may be understood functionally either as propagation, exacerbation, or compensation of such loss (Figure 1E). For instance, the functional effect of loss of 50% of the rod input may be propagated through the circuit, resulting in a loss of 50% of the retinal output. This would be evident as smaller responses (Figure 1E, curve 1) and/or maximum amplitude (Figure 1E, curve 2). If, on the other hand, the functional effect in the circuitry is exacerbated, then down-stream neurons will likely perform worse than input loss alone predicts. Alternatively, the functional effect of loss may be compensated for within the circuit, i.e., by an increase in gain, resulting in a restoration of the retinal output. Compensation would be evident as a response equal to (Figure 1E, curve 3) or even greater than that of control (Figure 1E, curve 4). We discriminate among these possibilities by using the well-defined retinal pathways to ganglion cells.

Rod-Mediated Charge and Spiking Output Recover Partially in Ganglion Cells after Rod Loss

To understand how rod pathways in mature retina react to the loss of half of their inputs, we measured the output of the retina by recording rod-mediated spikes from $A_{ON\text{-}S}$ ganglion cells. To stimulate rods, we presented flashes (10 ms) of blue light (470 nm) doubling in intensity from darkness. We used this stimulus in all experiments in which rods were preferentially stimulated. We recorded rod-mediated spike responses from control and Rho-DTR retina in cell-attached patch-clamp recordings (Figure 2A) and quantified responses by plotting the total number of spikes elicited by each flash intensity (Figure 2B). We fit these data with the Hill equation and used the fit parameters to compare responses from control and Rho-DTR retina (Figure 2C; Table S2). After the loss of 60% of rods, the rod-mediated spike response of $A_{ON\text{-}S}$ ganglion cells showed decreases in the maximum response (R_{max}) and in the light intensity at half the maximum response (I½). This indicates that, after partial rod loss, the rod-mediated response of $A_{ON\text{-}S}$ ganglion cells has fewer spikes but responds at lower light levels. Such results could be consistent with the propagation of reduced rod input through the circuit. However, the average loss of rod-mediated spikes (R_{max} reduced by 22%) is less than the average loss of rods (60%), suggesting that compensatory mechanisms in the mature retinal circuit act to mitigate the functional effects of rod loss. To understand the extent of this effect, we measured rod-mediated spikes in $A_{OFF\text{-}T}$ ganglion cells and found a similar mitigation of the effects of rod loss (Figure S3; Table S3). Furthermore, the increase in sensitivity of the rod-mediated spikes suggests that gain of function can occur after partial rod loss.

To understand how these spike responses are generated, we recorded the rod-mediated input currents onto $A_{ON\text{-}S}$ ganglion cells (Figures 2D and 2E). Excitatory current amplitude was unchanged, but the R_{max} of the integrated rod-mediated excitatory currents (charge transfer) was reduced after partial rod loss (Figure 2F; Table S2). This indicates that the amplitude or duration of rod responses are diminished. The reduced charge may explain the reduction in rod-mediated spikes that we observed. The charge transfer of rod-mediated inhibitory currents was not significantly different in the fit parameters between control and Rho-DTR retina (Figures 2G–2I; Table S2). This indicates that rod-mediated inhibitory currents onto $A_{ON\text{-}S}$ ganglion cells are unaffected by or have recovered from partial rod loss.

At Rod Light Levels, Intrinsic Excitability Is Maintained in $A_{ON\text{-}S}$ Ganglion Cells after Rod Loss

One possible cause of a decrease in rod-mediated spikes is a change in the current-to-spike transformation in the ganglion cell, i.e., intrinsic excitability. The transformation from currents to spikes includes voltage-gated conductances that are eliminated in the voltage-clamp recordings described above. Thus, to measure the current-to-spike gain in the cells for which intensity-response relationships were recorded for both spikes and currents, we calculated the ratio of the number of spikes to the peak charge elicited at each flash intensity (Figure 3A). A change in this ratio between control and Rho-DTR conditions would indicate that changes in voltage-gated conductances contribute to the observed decrease in spikes. We found no significant difference between the current-to-spike gain of cells from control and Rho-DTR retina at any of the flash intensities tested. This provides one line of evidence that compensation for input loss is not due to changes in the intrinsic excitability of $A_{ON\text{-}S}$ ganglion cells.

To further confirm that compensation occurs prior to the ganglion cell intrinsic excitability, we directly measured the current-to-spike transformation by injecting current into $A_{ON\text{-}S}$ ganglion cells in perforated patch-clamp configuration. This technique enables the simultaneous injection of a fluctuating white-noise current and measurement of the cell's spiking response (Kim and Rieke, 2001) (Figure 3B). To capture the current-to-spike transformation, we estimated the linear filter and nonlinearity that generated the spike response from the input current for each cell (Figure 3B, box). We found no significant differences in the linear filters or nonlinearities between cells from control and Rho-DTR retina in darkness, the condition that best simulates rod levels (linear filter: control versus Rho-DTR, $p = 0.522$; nonlinearity: control versus Rho-DTR, $p = 0.667$; control [Rho-DTR], $n = 19$ [20], permutation test). Both the current-to-spike ratio calculation and current injection support the conclusion that intrinsic excitability is maintained in $A_{ON\text{-}S}$ ganglion cells after rod loss. Thus, the site(s) of compensation are prior to the ganglion cell.

The Rod Bipolar Cell Is a Site of Compensation

Next, we examined other potential site(s) of compensation within the retinal circuit, upstream of $A_{ON\text{-}S}$ ganglion cells. For a population readout of photoreceptor and bipolar cell responses, we measured the electroretinogram (ERG) *in vivo* in control and Rho-DTR mice under dark-adapted (rod-mediated) conditions (Figure 4A). In Rho-DTR mice, we found a significant reduction in the a-wave amplitude of the dark-adapted ERG, a measure

proportional to the rod dark current. This finding indicates an overall decreased rod response in Rho-DTR retina (Figure 4B). In contrast, the amplitude of the b-wave, which is a measure proportional to the overall rod bipolar cell and Müller glia cell responses, had recovered at these same light levels 1 month after DT injection. The ratio between the a- and b-waves at a subsaturating light level (9.73 photons/μm^2/s) was significantly different in control and Rho-DTR mice ≥1 month after DT injection (1 month control [Rho-DTR]: 0.349 ± 0.091 [0.173 ± 0.073], mean ± SD, p = 0.009, t test; ≥ 4 months: 0.363 ± 0.075 [0.255 ± 0.090], p = 0.036, t test; Figure S6), demonstrating that the b-wave amplitude was greater than predicted from simple propagation of the a-wave amplitude loss. In contrast, this ratio between the a- and b-waves was not significantly different between control and Rho-DTR mice 3 days after DT injection, before rod death was complete (3 days: 0.276 ± 0.064 [0.242 ± 0.066], mean ± SD, p = 0.363, t test; Figure S6; STAR Methods), demonstrating that the reduction in b-wave amplitude was propagated from the reduction in the a-wave amplitude in the Rho-DTR mice. This indicates that, after 1 month, rod bipolar cell output can be maintained despite a decrease in rod input (Figure 4C). This finding suggests that compensation for rod loss occurs between the inner segment of the rods and the voltage output of the rod bipolar cells, which could include rod synaptic release, rod bipolar cell postsynaptic sites, and the current-to-voltage transformation within the rod bipolar cell.

The same mice were also stimulated under light-adapted (cone-mediated) conditions. In light-adapted conditions, in which the a-wave reflects cone activity and the b-wave reflects primarily ON cone bipolar cell responses, we observed no reduction in the amplitude of the a- or b-waves, indicating that population responses of cone photoreceptors and ON cone bipolar cells are not affected after 60% rod death (Figures 4D–4F).

Decreased Excitatory and Inhibitory Inputs to Rod Bipolar Cells Yield a Recovered Voltage Response

To further investigate whether compensation for rod loss occurs between the rod inner segments and the rod bipolar cell voltage output, we recorded directly from rod bipolar cells. We measured rod-mediated responses from rod bipolar cells in whole-cell current-clamp and voltage-clamp configurations (Figure 5). Recordings were made in the slice preparations and confirmed in whole-mount retina. Rod bipolar cells were identified by their location within the inner nuclear layer and ON light response in combination with polarity reversal at the reversal potential for excitatory currents. In contrast, ON cone bipolar cells had light responses that could not be reversed because of gap junctions (Veruki and Hartveit, 2002). The peak amplitude of the rod-mediated response was used to construct intensity-response relationships for individual rod bipolar cells. As described for the ganglion cells, these data were fit with the Hill equation and the parameters for the best-fit curves were used to compare across cells. After partial rod loss, we found no change in the peak amplitude of the voltage response of rod bipolar cells (Figures 5A–5C; Table S4). This aligns with results from the ERG and indicates that full compensation for the decreased rod input is achieved before the rod-mediated signal leaves the rod bipolar cell.

To understand how this voltage response is generated, we measured the excitatory (Figures 5D–5F) and inhibitory currents (Figures 5G–5I) onto rod bipolar cells under voltage clamp.

Following partial rod loss, we found a significant decrease in the R_{max} for both excitatory and inhibitory currents (Table S4). Excitatory currents were reduced on average by 53%, which reflects the percentage of rod loss. Inhibitory currents were reduced on average by 94%. The nearly complete loss of inhibition indicates that the effect of rod loss on inhibition is greater than the loss of excitatory input.

One explanation for the enhanced voltage response is that a compensatory mechanism is engaged to reduce inhibition in order to balance reduced excitation. Alternatively, these data may suggest that inhibition is stimulated in an all-or-nothing manner. In addition to a loss of input, partial rod death could also change the rod bipolar cell response to remaining rods. Such a change would be evident as an increase or decrease in sensitivity, represented by the I½ parameter. We found no change in the sensitivity of excitatory currents, which suggests that the remaining rod-to-rod bipolar cell synapses are unchanged, and that the site of compensation is the inhibitory currents. Anatomically, quantifications of rod bipolar cell synaptic ribbons and inhibitory postsynaptic puncta densities show no significant difference between control and Rho-DTR. Thus, physiological adaptive changes are not matched by anatomical synaptic changes in this case (Figure S4). Preliminary results show that the number of dendritic tips in rod bipolar cells is halved, suggesting the total membrane area of the rod bipolar cell has decreased and the input resistance has increased (Figure S5; Anastassov et al., 2019). An increase in resistance in Rho-DTR rod bipolar cells could contribute to the recovery of voltage output with diminished current input. Thus, we interpret that a reduction in inhibition potentially balances the reduction in excitation due to rod loss, allowing rod bipolar cells in Rho-DTR retina to generate voltage outputs comparable to control retina.

To summarize thus far, after 50%–60% rod death, the output of the rod population is reduced, and both excitation and inhibition onto rod bipolar cells are reduced. Consistent with the larger reduction in inhibition than in excitation, the voltage output of rod bipolar cells is maintained. The excitatory input onto $A_{ON\text{-}S}$ ganglion cells is thus partially recovered, which generates partially recovered spike responses to rod stimuli.

Cone-Mediated Charge and Spiking Output Increase in $A_{ON\text{-}S}$ Ganglion Cells after Rod Loss

In the primary rod pathway, rod-mediated signals reach ganglion cells via the axon terminals of ON cone bipolar cells (Figure 1A). Therefore, another possible site for signal amplification through the primary rod pathway is at the cone bipolar-to-ganglion cell synapse. To isolate this section of the circuit, we used a short-wavelength (S)-cone-preferring stimulus composed of flashes (10 ms) from a short-wavelength LED (370 nm) doubling in intensity on a blue mean to adapt rods. To understand whether signaling through the cone pathway is affected by partial rod loss, we recorded the cone-mediated spike response from $A_{ON\text{-}S}$ ganglion cells (Figures 6A–6C). We found significant increases in R_{max} and I½, as well as a decrease in the exponent in Rho-DTR retina (Table S5). This finding indicates that the cone-mediated spike response is increased in amplitude and decreased in sensitivity after rod loss, and more generally, that the loss of rods affects signaling through the cone pathway. To further investigate the source of this increased

spiking, we measured the cone-mediated excitatory (Figures 6D–6F) and inhibitory (Figures 6G–6I) currents onto $A_{ON\text{-}S}$ ganglion cells. We found that cone-mediated excitatory currents, similar to the cone-mediated spike output, showed an increase in R_{max} and decrease in the exponent (Table S5). Cone-mediated inhibitory currents showed no change after rod loss. This suggests that the increased spiking in response to cone-preferring stimuli may be driven by increased excitatory input from the ON cone bipolar to the ganglion cell. Alternatively, the loss of rods might directly affect cone signals (see Discussion).

We had previously eliminated the possibility that changes in intrinsic excitability in the $A_{ON\text{-}S}$ ganglion cells underlie changes in rod-mediated spikes. Here, we consider the possibility that retinal neurons are in a different light-adaptation state at cone light levels, thus explaining the increased spiking in $A_{ON\text{-}S}$ ganglion cells. We compared the ratio of cone-mediated spikes to excitatory current responses and found no significant differences between control and Rho-DTR conditions (Figure 6J). Furthermore, we injected white noise current with a rod-adapting mean to measure the intrinsic excitability of $A_{ON\text{-}S}$ ganglion cells for cone-mediated signals and found no change in either the linear filter or the nonlinearity after rod loss (Figure 6K; linear filter: control versus Rho-DTR, $p = 0.125$; nonlinearity: control versus Rho-DTR, $p = 0.410$; control [Rho-DTR] n = 12 [12]; permutation test). Both experiments demonstrate that the increased spiking does not arise from increased intrinsic excitability within the ganglion cell itself.

Partial Stimulation of Rods in Control Retina Does Not Mimic Rod-Mediated Light Responses after Partial Rod Death

We next aimed to understand whether the changes in $A_{ON\text{-}S}$ ganglion cell light responses after 50%–60% rod death were attributable to the propagation of lost input through the retinal circuit, mechanisms existing in control retina, and/or active compensation for lost input. To answer this question, we designed an experiment to measure the retinal response to 50% of inputs without the contribution of any circuitry changes, e.g., caused by cell death or prolonged deficit of input. Control cells were stimulated either fully with a spot of light or partially with only half of the spot on the cell's receptive field. The response to the half stimulus is a direct readout of 50% of inputs, thus providing a benchmark for what the light response in Rho-DTR retina might be if no compensatory mechanisms were active after the death of 50% of rods. Comparison of responses to the full and half stimulation against control and Rho-DTR retina reveals how the remaining partially deafferented circuit in Rho-DTR retina differs from control retina.

In the rod-mediated spike response to the half stimulus, we found a significant reduction in R_{max}, indicating a decrease in response amplitude, as well as an increase in I½, indicating a decrease in sensitivity (Figures 7A and 7B). R_{max} decreased on average by 49% and the sensitivity decreased on average by 52% (Table S6), suggesting that stimulating half of rods generates a proportional decrease in response amplitude and sensitivity. In contrast, in Rho-DTR retina, R_{max} of the rod-mediated spike response decreased by only 22%, suggesting that compensatory mechanisms have partially recovered the response after rod death. Furthermore, the sensitivity of the spike response decreased with half stimulation but increased in Rho-DTR retina, a further indication that the Rho-DTR light response is not

simply passive propagation of reduced rod stimulation. Since these rod-mediated responses to half stimulation of control retina differ from those in the Rho-DTR retina, these data demonstrate that stimulating half of the rods is functionally distinct from ablating half of the rods (Figure 7C).

Partial Stimulation of Cones Mimics Cone-Mediated Light Responses after Partial Rod Death

To understand whether the changes we observed in the cone-mediated light responses in Rho-DTR retina were attributable to existing mechanisms in control retina, rod death, and/or subsequent compensation, we presented cone-preferring stimuli in the full versus half conditions. To half stimulation, R_{max} and I½ of the cone-mediated spike response in control retina increased (Figures 7D and 7E; Table S6). This finding mimics the results from Rho-DTR retina, and therefore indicates that this increase in cone-mediated spiking is generated by a mechanism that is present in control retina and not a result of rod death. The half stimulation does not replicate the condition of 50% rod stimulation and 100% cone stimulation, which occurs with Rho-DTR retina, because cones can only be selectively stimulated with the rod-adapting background. Instead, the half stimulation achieves 50% rod stimulation and 50% cone stimulation. Despite this partial stimulation of cones, the results from half stimulation match the results from Rho-DTR retina (Figure 7F). In erring on the side of less cone stimulation than occurs in Rho-DTR retina, we are unable to draw conclusions about the magnitude of this result, but we are able to conclude that cone-mediated signaling increases in the half stimulation condition. Results show that cone-mediated spiking in $A_{ON\text{-}S}$ ganglion cells is enhanced with partial stimulation, similarly to partial rod death. These findings demonstrate that mechanisms that enhance cone-mediated signaling exist in control retina and are independent of compensation within the rod pathway after partial rod death.

DISCUSSION

To understand the functional impact of primary neuron death on the mature circuit requires control over the timing and extent of death. In this study, we induced death of approximately half of the rods after development (Figure 1) and recorded light responses throughout the circuit. At the output of the retina in ganglion cells, we found partial recovery of excitatory current charge and the number of spikes elicited by rod stimuli (Figure 2), which was not accounted for by the intrinsic excitability of these cells (Figure 3). While output of rods is reduced by a degree consistent with rod loss, rod bipolar cell output is reduced less than predicted by the reduction in rod responses (Figure 4). These results suggest that recovery happens between the rod and rod bipolar cell output. Direct recordings from rod bipolar cells indicated that decreased excitatory and inhibitory currents may balance to generate recovered voltage responses (Figure 5). To probe the circuitry components that are part of both the primary rod pathway and the cone pathway, we measured ganglion cell light responses to cone stimuli and found an increase in cone-mediated spiking, driven by increased excitatory current charge and not by amplification in intrinsic excitability (Figure 6). Finally, half stimulation of control retina revealed circuit changes different from those observed after half ablation of rods. We demonstrated that the changes in cone-mediated

light responses after death of half of the rods in Rho-DTR retina are similar to those that occur with stimulation of half of photoreceptors in control retina, indicating that the cone pathway withstands partial rod death. In contrast, we demonstrated that rod-mediated light responses in Rho-DTR retina differ from those that occur with half stimulation of control retina, indicating that after rod death the mature retina engages *de novo* mechanisms to restore functional output (Figure 7).

Effects of Cell Death on the Resting Activity in the Deafferented Circuit

One question is whether rod death in the mature retina could be comparable to raising the background light level in control retina because, presumably, the overall resting glutamate release has decreased following partial rod loss. In one respect, in Rho-DTR retina, ganglion cells exhibit faster responses consistent with light-adapted retina; however, in another respect, their sensitivity is increased rather than decreased, inconsistent with light-adapted retina. This increase in sensitivity can be accounted for by decreased inhibition onto rod bipolar cells, which acts as a compensatory mechanism for rod loss. Taken together, these results strongly suggest that the compensation mechanism after rod death is distinct from those responsible for adaptation. Below, we discuss these effects.

An important feature of circuit function is the resting neurotransmitter release, which sets the state of the circuit. Ablation can change this state. In partial ablation of the vestibular system, resting activity was reduced after deafferentation (Shimazu and Precht, 1966; Hoshino and Pompeiano, 1977). Similarly, in our study, we speculate how resting glutamate release by photoreceptors, which contributes to the retina's adaptation state, is disrupted after partial rod ablation. The half stimulation experiment can distinguish between some of the effects of partial stimulation and partial ablation; however, we acknowledge how the effects of stimulation and ablation may be different. The half stimulation of control retina and half rod ablation in the Rho-DTR have distinct consequences that allow us to draw conclusions about the partially deafferented circuit. We compare three conditions: (condition 1) full stimulation of control retina, (condition 2) half stimulation of control retina, and (condition 3) full stimulation of Rho-DTR retina. We consider rod-mediated, then cone-mediated light responses.

In signaling rod-mediated light responses on a dark background, Rho-DTR is missing rods that would otherwise convey resting activity, i.e., signaling darkness, to the retina. As a prediction, the Rho-DTR (condition 3) would be light-adapted compared to half stimulation of control retina (condition 2), because only half the resting activity is being conveyed by the remaining rods. As signatures of a light-adapted retina, the Rho-DTR (condition 3) neurons would be expected to have faster and less sensitive responses. Indeed, ganglion cells in Rho-DTR have rod-mediated responses faster than in control retinas, indicative of a light-adapted retina. However, Rho-DTR ganglion cells have rod-mediated responses that are more, rather than less, sensitive, indicating that compensatory mechanisms other than light adaptation are engaged.

For cone-mediated light responses on a mean background, full stimulation of control retina has the full complement of rods stimulated by the mean background (condition 1), i.e., most light-adapted. Half stimulation of control retina has half of rods stimulated by the mean

background, while the other half of rods signals darkness (condition 2), i.e., least light-adapted. In between these extremes, Rho-DTR retina are missing rods that would signal the mean background, i.e., the retina signals less light than is presented (condition 3). Indeed, ganglion cells in the full stimulation (condition 1) have lower sensitivities and faster responses, both signatures of light-adapted retina. In contrast, ganglion cells in both the half stimulation (condition 2) and Rho-DTR (condition 3) have greater sensitivities and qualitatively slower responses, both signatures of dark-adapted retina. In addition, ganglion cell responses in Rho-DTR (condition 3) show greater sensitivity than those in half stimulation (condition 2), despite the expectation that Rho-DTR is more light-adapted, providing further evidence for compensatory mechanisms that are invoked by ablation but not by half stimulation.

Influence of Input Loss on Sites of Compensation

Classic studies of the deafferented circuit have been done in the lesioned vestibular system and found compensation in vestibulo-ocular and vestibulo-spinal functions for input lost after removal of one vestibular labyrinth (Precht, 1986). Following input loss, inhibition is decreased in the vestibular system (Shimazu and Precht, 1966; Markham et al., 1977). Previous work in visual cortex has also demonstrated that inhibitory circuits exhibit more structural plasticity than excitatory circuits after monocular deprivation (Villa et al., 2016). Similarly, our findings localize the site of compensation for input loss to the inhibitory currents onto the rod bipolar cell. Rod bipolar cells have excitatory currents reduced by 53%, and inhibitory currents reduced by 94%. The recovery of voltage responses could result from the rod bipolar cell losing part of its dendritic tree, becoming more electrically compact, increasing its input resistance, and thus enabling a smaller current to produce a voltage response comparable to control conditions. The end result is that more distal sites of compensation in the rod pathway are obviated by recovery at the rod bipolar cell voltage.

Our previous study on partial cone loss revealed that inhibitory surrounds of $A_{ON\text{-}S}$ ganglion cells expanded, while excitatory centers of these same cells shrank, indicating not only that the inhibitory surround is affected by partial cone loss, but that it may also be a site of compensation for input loss (Care et al., 2019). In contrast to these findings, the present study demonstrates the inhibitory circuits onto ganglion cells remain relatively stable. The difference between our previous study with cone ablation and present study with rod ablation could be the relatively greater photoreceptor loss with rods, i.e., 50% of total photoreceptors, compared with cones, i.e., 1.5% of total photoreceptors. We speculate that the degree of input loss may determine the site of compensation. With less input loss, as was the case after partial cone ablation, the site of compensation is late in the circuit because such mild deficits require greater convergence between the input and postsynaptic cell to detect, i.e., greater spatial integration. With greater input loss, as demonstrated in this study with partial ablation of rods, the site of compensation can be earlier in the circuit because major deficits require less convergence between the input and postsynaptic cell to detect, i.e., less spatial integration. Multiple sites of compensation harken back to our understanding of multiple sites of gain control that operate under different light levels: at dim light levels, gain control occurs later in the circuit between secondary and tertiary neurons; for brighter light levels, gain control occurs earlier in the circuit at primary sensory receptors (Dunn et

al., 2006; 2007). Perhaps similar distributed compensatory mechanisms at multiple sites are engaged after varying degrees of input loss.

Implications for Neurodegenerative Diseases, Acute Loss of Sensory Input, and Earlier Diagnosis

Acute ablation of rod photoreceptors in mature retina can mimic the degree of photoreceptor loss at a specific time point in genetic diseases broadly classified as retinitis pigmentosa in which rods die for various reasons; however, our method of ablation did not mimic the degenerative aspects of these diseases. At intervals of ≥4 months since ablation, the remaining rod population remained stable and initial rod death did not induce further rod loss (Table S7). In this regard, acute rod ablation cannot mimic progressive degeneration, yet perhaps we can garner insight from results reported here. First, the relative stability of secondary neurons upon ablation of primary sensory receptors in a mature circuit is consistent with observations in the auditory system upon ablation of mature hair cells (Tong et al., 2015; Kurioka et al., 2016). Such insight provides promise for therapeutics that capitalize on existing circuits, e.g., electrical stimulation of or genetically engineering light sensitivity into the surviving neurons (reviewed in Wood et al., 2019). Second, as discussed below, the physiological state of a circuit with half its sensory receptors appears distinct in ways that diagnostic tests could capitalize upon.

Our work provides evidence for the independence of rod and cone pathways despite convergence at the cone bipolar-to-ganglion cell synapse. When rods are ablated, cone-mediated responses in ganglion cells in control retina can be mimicked with half stimulation, i.e., the cone pathway remains intact. Such findings, alongside evidence for compensation within the deafferented circuit, may explain why photoreceptor degeneration evades detection both by the patient reporting vision loss and by diagnostics of visual sensitivity and acuity (Ratnam et al., 2013). Greater than half of the cones must be missing before visual deficits start to present clinically. Commonly used tests for visual sensitivity and acuity are conducted at a single background light level. In our simulation of photoreceptor loss by partial stimulation, we have uncovered how the deafferented retinal circuit, while generally functional, differs from that of an unperturbed retina. One prediction is that at a single background, changes in kinetics and sensitivity following photoreceptor loss may be subtle enough to be mistaken for normal. However, if threshold detection is measured at multiple backgrounds, photoreceptor loss may present as kinetic or sensitivity changes that are consistent with a more light-adapted state than expected in unperturbed retina. Consistent with this prediction, the electrical response filter, i.e., spike triggered average, of ganglion cell responses to electrical stimulation in *rd10* retina, a model of rod degeneration, is faster as if light-adapted compared to the control ganglion cells (Sekhar et al., 2017). Whether the light-adapted state can be used as a diagnostic tool requires that the rest of the visual system has not masked changes at the level of the retina or that the method of testing isolates retinal responses, e.g., electroretinogram. The present study has the potential to link mechanistic insight gained from mouse retina to clinically relevant efforts to create diagnostic tests for earlier detection of photoreceptor loss.

STAR★METHODS

RESOURCE AVAILABILITY

Lead Contact—Further information and requests for resources and reagents should be directed to and will be fulfilled by the Lead Contact, Felice Dunn (Felice.Dunn@ucsf.edu).

Materials Availability—Unique reagents generated in this study are available upon request with a completed Materials Transfer Agreement.

Data and Code Availability—The code generated during this study for image analysis are available at https://lucadellasantina.github.io/ObjectFinder/

The code generated during this study for physiology analysis is available upon request.

The datasets supporting the current study are available upon request.

EXPERIMENTAL MODEL AND SUBJECT DETAILS

Mice—All procedures were done in accordance with the University of California, San Francisco Institutional Animal Care and Use protocols. The following transgenic mouse lines were crossed: *Rho-iCre* (Li et al., 2005) for Cre-recombinase expression in rods and *Rosa26-loxP-stop-loxP-DTR* (Buch et al., 2005) for Cre-dependent expression of the simian diphtheria toxin receptor. When crossed to a fluorescent reporter line *Ai6* (Madisen et al., 2010), the *Rho-iCre* revealed high specificity to the rod population, with no cone pedicles and extremely rare cell bodies in the inner nuclear layer and ganglion cell layer labeled (Figure S2). These transgenic mice were back-crossed into the *C57BL/6J* background. Male and female mice were used for experiments. Diphtheria toxin injections were done between P30–40 at dosages of 100ng/g for 2 injections administered 7 days apart (Care et al., 2019). Mice injected with an equivalent volume of saline were used as littermate controls. Quantification of rod loss demonstrates uniform 50–60% rod loss across each section. All experiments in the main figures were conducted 1 month after DT injection. Two additional cohorts of mice were examined: (1) one at 3 days after the second DT injection revealed < 10% rod death by this time point (number of rows of cell bodies in the ONL was significantly lower after DT injection: control [DTR] = 11 ± 0.67; number of observations and animals: 12 and 6 [10 ± 2; number of observations and animals: 14 and 7], median ± IQR, $p = 0.0037$, rank sum test; but not significantly different in the number of rows in the INL: control [DTR] = 4.67 ± 0.33 [4.33 ± 0.67] median ± IQR, $p = 0.101$, rank sum test; data not shown), and (2) another at ≥ 4 months after DT injection that revealed rod death remains at 50–60%, but there are further changes to the bipolar cell responses (Figures S6 and S7; Table S7). In this ablation system, rod death reaches an asymptote between 3 to 30 days following DT injection.

METHOD DETAILS

Tissue preparation for immunostaining—Immunostaining protocols were identical to those described previously (Care et al., 2019). Reagents are listed in the Key Resources Table.

Quantification of cell death—To count photoreceptor and interneuron cell bodies, sample preparations were identical to those described previously (Care et al., 2019).

Electrophysiology tissue preparation—Procedures for the flat mount preparation of recording from alpha ON-sustained ganglion cells (abbr. $A_{ON\text{-}S}$ ganglion cells) (Bleckert et al., 2014) and rod bipolar cells were identical to those described previously (Care et al., 2019). Recordings were done in ventral-nasal retina where the largest of the $A_{ON\text{-}S}$ ganglion cells reside and where short (S)-wavelength sensitive opsin dominates.

Procedures for slice preparation for recording from rod bipolar cells were similar to those described previously (Dunn et al., 2006). Briefly, the isolated retina was embedded in 3% low melting agar in oxygenated HEPES buffered Ames and sliced at 200μm sections on a Vibratome 1200S (Leica). Slices were chosen based on the accessibility of the rod bipolar cells and the intactness of the entire section.

Patch-clamp recordings—Patch-clamp recordings from ganglion cells were identical to those described previously (Care et al., 2019). Patch-clamp recordings from rod bipolar cells were made with electrodes pulled from borosilicate glass (Sutter Instruments) on a DMZeitz to 10–15 MOhm resistance. The electrode internal solution was either cesium methane sulfonate (Care et al., 2019) or potassium aspartate containing (in mM): 125 potassium aspartate, 1 MgCl, 10 KCl, 1CaCl, 10 HEPES, 2 EGTA, 4 ATP, 0.5 GTP, adjusted to pH 7.2 with KOH, adjusted to 273–279 mosm with potassium aspartate, and 0.04% Lucifer Yellow dye. For perforated patch-clamp recordings in Figures 3 and 6, amphotericin-B (0.05 mg/ml) was added to the potassium aspartate internal solution in the back portion, but not the front tip, of the electrode.

Cell identification—Identification of $A_{ON\text{-}S}$ ganglion cells included sustained spiking response to a 500ms light step and immunolabeling described in previously (Care et al., 2019).

Rod bipolar cells were targeted by the soma location in the outermost layer of the inner nuclear layer, next to the outer plexiform layer. Identification of rod bipolar cells included ON light responses that could be reversed at positive holding potentials and immunolabeling that revealed large axon terminals in the innermost layer of the inner plexiform layer and colocalization with protein kinase C alpha (PKCalpha).

Light stimuli—Light stimuli were generated by three LEDs with single peaks at 390nm, 405nm, and 470nm. For rod-mediated stimuli, a 10ms flash of the 470nm was presented on a dark background. For cone-mediated stimuli, a 10ms flash of the 370nm or 405nm LEDs was presented on a mean background of 4000 rod isomerizations per rod per second (Rh*/rod/sec) with the 470nm LED to adapt the rods. The stimuli were presented through a circular aperture 900 μm in diameter. For partial stimulation, this spot was displaced so that approximately half of the spot was on the ganglion cell's receptive field.

Electroretinogram recordings—Procedures for the electroretinograms (ERGs) were identical to those described previously (Care et al., 2019) with the following differences.

Diagnosys LLC is located in Lowell, MA. The b-wave amplitude was measured from the peak of the a-wave to the second highest positive peak because oscillatory potentials occur during the b-wave. The a-wave to b-wave ratio was measured as the ratio between the amplitude of a-wave and the amplitude of b-wave in response to a flash of 9.73 photons*μm $^{-2}$*s^{-1}, at which the b-wave amplitude of dark-adapted ERG approaches saturation (Perlman, 1983).

QUANTIFICATION AND STATISTICAL ANALYSIS

Quantification of intensity response relationships—Responses of each cell were measured 5–10 times at each light level. Analysis parameters (number of spikes, peak current amplitude, charge) were measured for each individual response and averaged at each light level within each cell. For each cell, these averages were plotted against the light intensity which elicited the response and the resulting plot was fit with the Hill equation in Igor Pro:

$$fit = base + \frac{R_{max} - base}{1 + \left[\frac{x_{half}}{x}\right]^{Exp}}$$

The parameters of this fit included the baseline (base), maximum (referred to as R_{max}), Exponent (referred to as Exp), intensity at half maximum (referred to as I½) are shown as histograms in Figures 2, 5, and 6. The intensity at half maximum is referred to as "sensitivity" though we only accounted for the average, and not variability, in the responses. To construct the average intensity response plots in panels B, E, and H of these figures, as well as the left side of Figures 7B and 7E, the average intensity response plots generated for each cell were averaged before the Hill equation fit. Points at light intensities within 30% of each other were combined (shown with horizontal error bars which are smaller than the point marker in most cases).

Linear-Nonlinear Filters—To determine the intrinsic excitability of $A_{ON\text{-}S}$ ganglion cells, we made perforated current-clamp recordings as described above. After establishing access, either the background was kept dark (Figure 3) or rods were adapted down with a constant blue mean at 4000 Rh*/rod/sec (Figure 6). White noise current was injected with a 1000 Hz frequency cutoff and 500pA standard deviation with an upper and lower limit of ± 200pA. The standard deviation was determined empirically to obtain a full input-output function. The mean was at 0 pA unless holding current was required to keep spontaneous spiking less than 1 Hz and to keep the resting membrane potential at approximately −60mV.

To calculate the linear filter we followed Baccus and Meister (Baccus and Meister, 2002). Briefly, the linear filter, F(t), was the correlation of the stimulus, s(t), and the response, r(t), normalized by the autocorrelation of the stimulus. To then calculate the nonlinear response function, N(g), we convolved the stimulus with the linear filter, to get the generator potential g(t), which was then plotted against r(t), averaging over values of r over bins of g containing an equal number of points. The nonlinearity was fit with a sigmoid function:

$$fit = base + \frac{max}{1 + e\left[\frac{x_{half} - x}{rate}\right]}$$

Linear filters and nonlinearities from control and DTR conditions were compared by a permutation test (p values reported in Results section describing Figures 3 and 6).

Statistical analysis—In the histograms, medians are indicated by arrowheads. To identify significant differences between conditions, a Wilcoxon rank sum test (abbr. rank sum) was used for Figures 1–6, and a Wilcoxon sign rank test (abbr. sign rank) was used for paired data (Figure 7). A permutation test was used to compare linear-nonlinear filters (Figures 3 and 6). The permutation test took the root mean squared difference between the average of the populations. This difference was compared to random chance by permuting the categories of cells to form two populations 10,000 times and calculating the root mean squared difference. The differences from the actual and permuted populations were compared to determine the p values. All p values are indicated in the Results. Asterisks in Figures indicate the following p values: * ≤ 0.05, ** ≤ 0.01, *** ≤ 0.005.

Supplementary Material

Refer to Web version on PubMed Central for supplementary material.

ACKNOWLEDGMENTS

We thank Jenita Ngo, Suling Wang, and Connie Chen for technical assistance and David Copenhagen, Jacque Duncan, Scott Harris, Jonathan Horton, Jeanette Hyer, Yvonne Ou, Manuel Soliño, Michael Stryker, and Alfred Yu for helpful discussions. This work was supported by NIH through Grants T32EY007120, F31EY028017 (R.A.C.), EY030136 (F.A.D.), and Vision Core Grant P30 EY002162 (UCSF), and by foundation grants from McKnight Foundation, Research to Prevent Blindness (Unrestricted Grant), and That Man May See.

REFERENCES

Anastassov IA, Wang W, and Dunn FA (2019). Synaptogenesis and synaptic protein localization in the postnatal development of rod bipolar cell dendrites in mouse retina. J. Comp. Neurol 527, 52–66. [PubMed: 28547795]

Atick JJ, and Redlich AN (1990). Towards a theory of early visual processing. Neural Comput. 2, 308–320.

Baccus SA, and Meister M (2002). Fast and slow contrast adaptation in retinal circuitry. Neuron 36, 909–919. [PubMed: 12467594]

Barlow HB (1953). Summation and inhibition in the frog's retina. J. Physiol 119, 69–88. [PubMed: 13035718]

Beier C, Hovhannisyan A, Weiser S, Kung J, Lee S, Lee DY, Huie P, Dalal R, Palanker D, and Sher A (2017). Deafferented adult rod bipolar cells create new synapses with photoreceptors to restore vision. J. Neurosci 37, 4635–4644. [PubMed: 28373392]

Bleckert A, Schwartz GW, Turner MH, Rieke F, and Wong ROL (2014). Visual space is represented by nonmatching topographies of distinct mouse retinal ganglion cell types. Curr. Biol 24, 310–315. [PubMed: 24440397]

Buch T, Heppner FL, Tertilt C, Heinen TJAJ, Kremer M, Wunderlich FT, Jung S, and Waisman A (2005). A Cre-inducible diphtheria toxin receptor mediates cell lineage ablation after toxin administration. Nat. Methods 2, 419–426. [PubMed: 15908920]

Care RA, Kastner DB, De la Huerta I, Pan S, Khoche A, Della Santina L, Gamlin C, Santo Tomas C, Ngo J, Chen A, et al. (2019). Partial cone loss triggers synapse-specific remodeling and spatial receptive field rearrangements in a mature retinal circuit. Cell Rep. 27, 2171–2183.e5. [PubMed: 31091454]

Della Santina L, Inman DM, Lupien CB, Horner PJ, and Wong ROL (2013). Differential progression of structural and functional alterations in distinct retinal ganglion cell types in a mouse model of glaucoma. J. Neurosci 33, 17444–17457. [PubMed: 24174678]

Dunn FA, Doan T, Sampath AP, and Rieke F (2006). Controlling the gain of rod-mediated signals in the Mammalian retina. J. Neurosci 26, 3959–3970. [PubMed: 16611812]

Dunn FA, Lankheet MJ, and Rieke F (2007). Light adaptation in cone vision involves switching between receptor and post-receptor sites. Nature 449, 603–606. [PubMed: 17851533]

Hoshino K, and Pompeiano O (1977). Crossed responses of lateral vestibular neurons to macular labyrinthine stimulation. Brain Res. 131, 152–157. [PubMed: 884540]

Jeon CJ, Strettoi E, and Masland RH (1998). The major cell populations of the mouse retina. J. Neurosci 18, 8936–8946. [PubMed: 9786999]

Kerschensteiner D, Morgan JL, Parker ED, Lewis RM, and Wong ROL (2009). Neurotransmission selectively regulates synapse formation in parallel circuits in vivo. Nature 460, 1016–1020. [PubMed: 19693082]

Kim KJ, and Rieke F (2001). Temporal contrast adaptation in the input and output signals of salamander retinal ganglion cells. J. Neurosci 21, 287–299. [PubMed: 11150346]

Krieger B, Qiao M, Rousso DL, Sanes JR, and Meister M (2017). Four alpha ganglion cell types in mouse retina: function, structure, and molecular signatures. PLoS ONE 12, e0180091. [PubMed: 28753612]

Kuffler SW (1953). Discharge patterns and functional organization of mammalian retina. J. Neurophysiol 16, 37–68. [PubMed: 13035466]

Kurioka T, Lee MY, Heeringa AN, Beyer LA, Swiderski DL, Kanicki AC, Kabara LL, Dolan DF, Shore SE, and Raphael Y (2016). Selective hair cell ablation and noise exposure lead to different patterns of changes in the cochlea and the cochlear nucleus. Neuroscience 332, 242–257. [PubMed: 27403879]

Li S, Chen D, Sauvé Y, McCandless J, Chen Y-J, and Chen C-K (2005). Rhodopsin-iCre transgenic mouse line for Cre-mediated rod-specific gene targeting. Genesis 41, 73–80. [PubMed: 15682388]

Madisen L, Zwingman TA, Sunkin SM, Oh SW, Zariwala HA, Gu H, Ng LL, Palmiter RD, Hawrylycz MJ, Jones AR, et al. (2010). A robust and high-throughput Cre reporting and characterization system for the whole mouse brain. Nat. Neurosci 13, 133–140. [PubMed: 20023653]

Margolis DJ, and Detwiler PB (2007). Different mechanisms generate maintained activity in ON and OFF retinal ganglion cells. J. Neurosci 27, 5994–6005. [PubMed: 17537971]

Markham CH, Yagi T, and Curthoys IS (1977). The contribution of the contralateral labyrinth to second order vestibular neuronal activity in the cat. Brain Res. 138, 99–109. [PubMed: 589471]

Murphy GJ, and Rieke F (2006). Network variability limits stimulus-evoked spike timing precision in retinal ganglion cells. Neuron 52, 511–524. [PubMed: 17088216]

Perlman I (1983). Relationship between the amplitudes of the b wave and the a wave as a useful index for evaluating the electroretinogram. Br. J. Ophthalmol 67, 443–448. [PubMed: 6602626]

Precht W (1986). Recovery of some vestibuloocular and vestibulospinal functions following unilateral labyrinthectomy. Prog. Brain Res 64, 381–389. [PubMed: 3523608]

Ratnam K, Carroll J, Porco TC, Duncan JL, and Roorda A (2013). Relationship between foveal cone structure and clinical measures of visual function in patients with inherited retinal degenerations. Invest. Ophthalmol. Vis. Sci 54, 5836–5847. [PubMed: 23908179]

Sekhar S, Jalligampala A, Zrenner E, and Rathbun DL (2017). Correspondence between visual and electrical input filters of ON and OFF mouse retinal ganglion cells. J. Neural Eng 14, 046017. [PubMed: 28489020]

Shen N, Wang B, Soto F, and Kerschensteiner D (2020). Homeostatic Plasticity Shapes the Retinal Response to Photoreceptor Degeneration. Current Biology 30, 1916–1926. [PubMed: 32243858]

Sher A, Jones BW, Huie P, Paulus YM, Lavinsky D, Leung L-SS, Nomoto H, Beier C, Marc RE, and Palanker D (2013). Restoration of retinal structure and function after selective photocoagulation. J. Neurosci 33, 6800–6808. [PubMed: 23595739]

Shimazu H, and Precht W (1966). Inhibition of central vestibular neurons from the contralateral labyrinth and its mediating pathway. J. Neurophysiol 29, 467–492. [PubMed: 5961161]

Tong L, Strong MK, Kaur T, Juiz JM, Oesterle EC, Hume C, Warchol ME, Palmiter RD, and Rubel EW (2015). Selective deletion of cochlear hair cells causes rapid age-dependent changes in spiral ganglion and cochlear nucleus neurons. J. Neurosci 35, 7878–7891. [PubMed: 25995473]

van Wyk M, Wässle H, and Taylor WR (2009). Receptive field properties of ON- and OFF-ganglion cells in the mouse retina. Vis. Neurosci 26, 297–308. [PubMed: 19602302]

Veruki ML, and Hartveit E (2002). Electrical synapses mediate signal transmission in the rod pathway of the mammalian retina. J. Neurosci 22, 10558–10566. [PubMed: 12486148]

Villa KL, Berry KP, Subramanian J, Cha JW, Chan Oh W, Kwon H-B, Kubota Y, So PTC, and Nedivi E (2016). Inhibitory synapses are repeatedly assembled and removed at persistent sites in vivo. Neuron 90, 662–664.

Wood EH, Tang PH, De la Huerta I, Korot E, Muscat S, Palanker DA, and Williams GA (2019). Stem cell therapies, gene-based therapies, optogenetics, and retinal prosthetics: current state and implications for the future. Retina 39, 820–835. [PubMed: 30664120]

Highlights

- Mature retina recovers functionally from loss of half of rod primary sensory neurons
- Reduced inhibition at secondary neurons functionally compensates for excitation loss
- Compensation from rod loss is not recapitulated by half stimulation of control retina
- Although using the same output neuron, the cone pathway withstands loss of half of rods

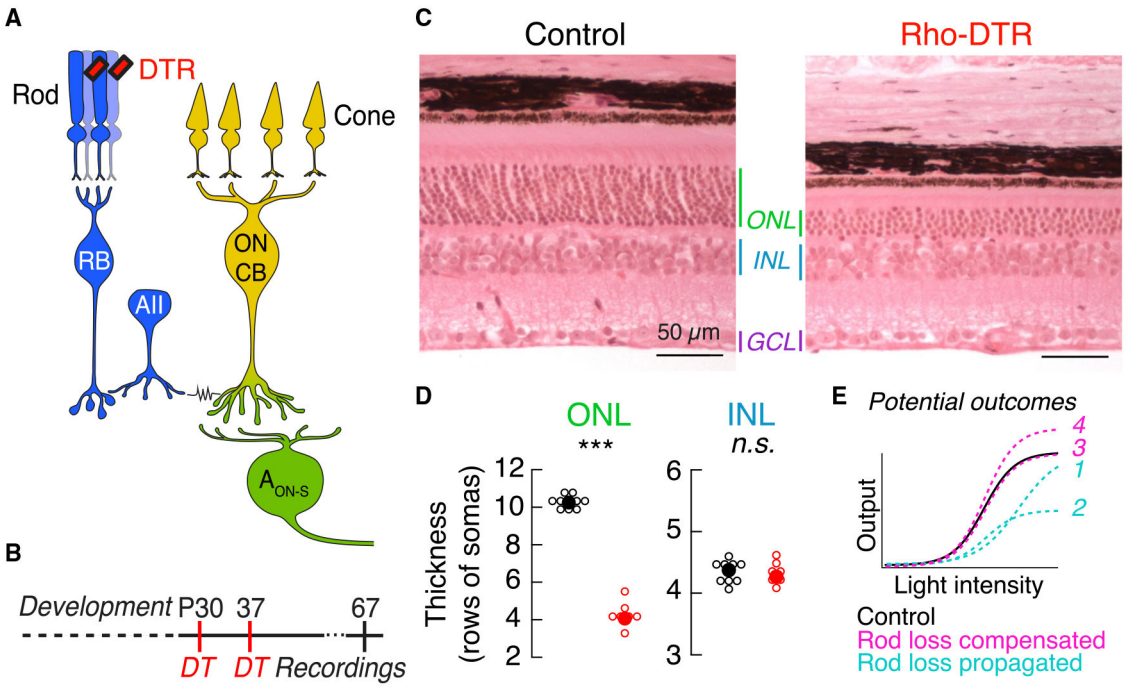

Figure 1. Diphtheria Toxin Receptor System Ablates Half the Rod Population while Preserving Inner Retinal Neurons in Adult Mice

(A) Schematic of the primary rod bipolar cell pathway: rod → rod bipolar cell (RB) → AII amacrine cell (AII) → ON cone bipolar cell (ON CB) → ganglion cell, including the alpha ON sustained ganglion cell ($A_{ON\text{-}S}$). Rod-mediated signals (blue) and cone-mediated signals (yellow) converge at the synapses between ON cone bipolar cells and ganglion cells (green). Red rectangles indicate the expression of the simian diphtheria toxin receptor (DTR) driven under the promoter for rhodopsin and selectively expressed in rods. Cartoons of the rod and cone photoreceptors are used in subsequent figures to denote the photoreceptor pathway stimulated, and cartoons of the rod bipolar and ganglion cells are used to denote the cell type recorded.

(B) Time course of diphtheria toxin (DT) injection at postnatal day 30 (P30) and a second injection at P37 allows the retina to develop before ablation of rods. Data in main figures acquired 1 month after the second DT injection.

(C) Retinal sections stained with hematoxylin and eosin in control (left) and Rho-DTR (right) conditions. Select retinal layers are labeled: outer nuclear layer (ONL) containing 97.2% rods (Jeon et al., 1998), inner nuclear layer (INL) containing bipolar and amacrine cell bodies, and the ganglion cell layer (GCL) containing displaced amacrine and ganglion cell bodies.

(D) Quantification of the number of cell bodies in each column of the ONL and INL for control (black) and Rho-DTR (red) conditions. The number of cell bodies is only significantly different in the ONL (asterisks represent significant p values by the rank sum test). Points are median ± IQR.

(E) Schematic of an ideal intensity-response relationship for light stimuli and functional responses of retinal neurons. If the effects of rod ablation are propagated through the retinal circuit, then light responses postsynaptic to the rod could exhibit loss of inputs, e.g., smaller

responses (curves 1 or 2). If, however, the effects of rod ablation are partially or fully compensated by postsynaptic neurons, then light responses postsynaptic to the rod could exhibit partial or full recovery, e.g., response that is greater than predicted based on the degree of rod loss (curves 3 or 4).

See also Figures S1, S2, and S7, and Tables S1 and S7.

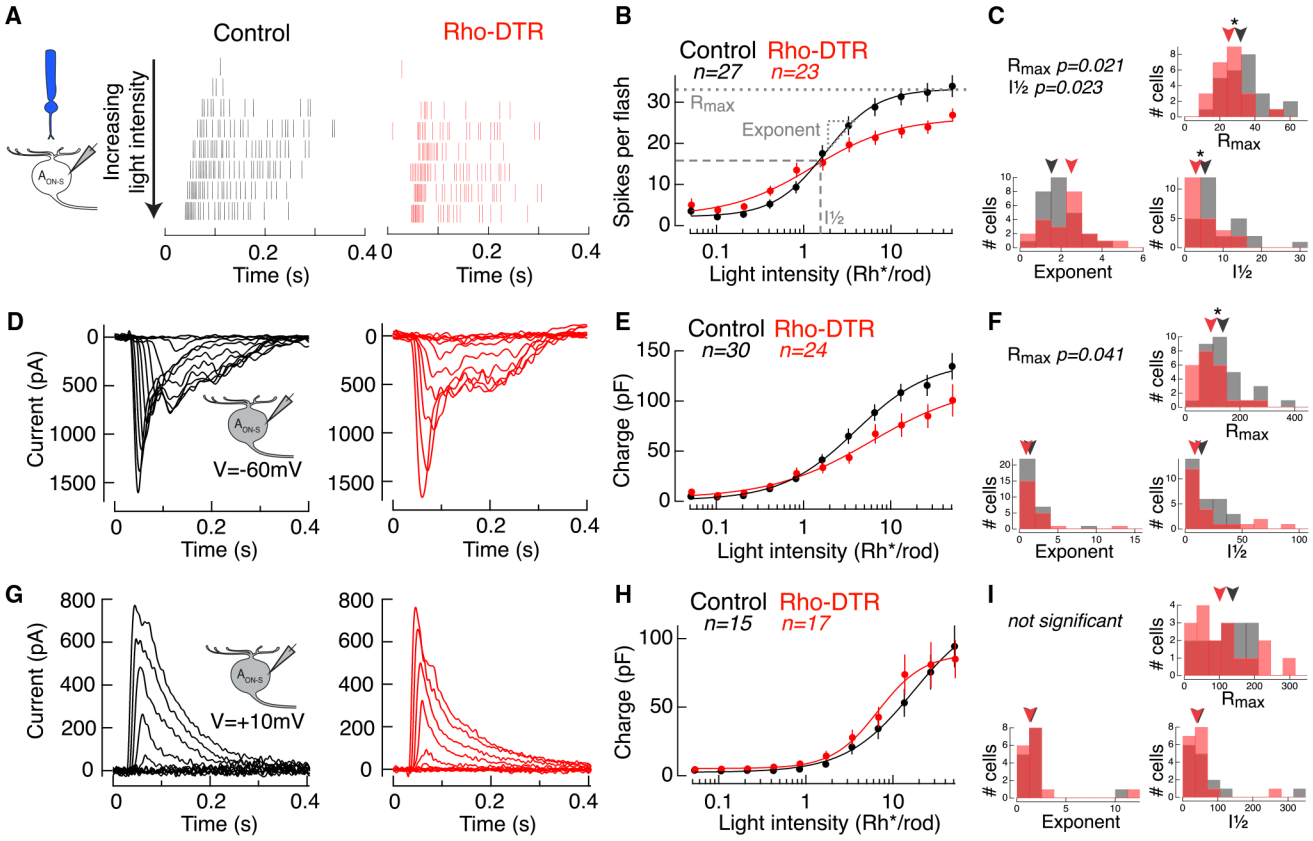

Figure 2. Rod-Mediated Light Responses in A_{ON-S} Ganglion Cells Have Partially Recovered Excitatory Currents and Spike Output

(A) Spike rasters from cell-attached recordings of A_{ON-S} ganglion cells in response to a rod-preferring stimulus: 10-ms flash at time 0 with the 470-nm LED on a dark background. Each row shows the response to a flash doubling in intensity from top to bottom in control (black) and Rho-DTR (red) conditions.

(B) Average intensity-response relationship for the total number of spikes in response to each flash intensity. Points are mean ± SEM, n is number of cells. (B, E, and H) Data points fit with a Hill equation, which can be captured by a maximum response (R_{max}), intensity at half maximum response (I½), and exponent.

(C) Histogram of three fit parameters for the population of A_{ON-S} ganglion cells in control and Rho-DTR conditions. (C, F, and I) Triangles above represent the median of each distribution, and asterisks denote significant differences between control and Rho-DTR populations by the rank sum test. Significant p values are reported in the upper left corner.

(D) Excitatory currents from voltage-clamp recordings of A_{ON-S} ganglion cells (V = −60 mV) in response to the same rod-mediated stimulus described above.

(E) Intensity-response relationship for the integral of the excitatory current.

(F) As described above for fits to the excitatory charge for individual cells.

(G) Inhibitory currents from voltage-clamp recordings of A_{ON-S} ganglion cells (V = +10 to +60 mV, determined by reversal of the light response) in response to the same rod-mediated stimulus described above.

(H) Intensity-response relationship for the integral of the inhibitory current.

(I) As described above for fits to the inhibitory charge for individual cells. See also Figure S3 and Tables S2 and S3.

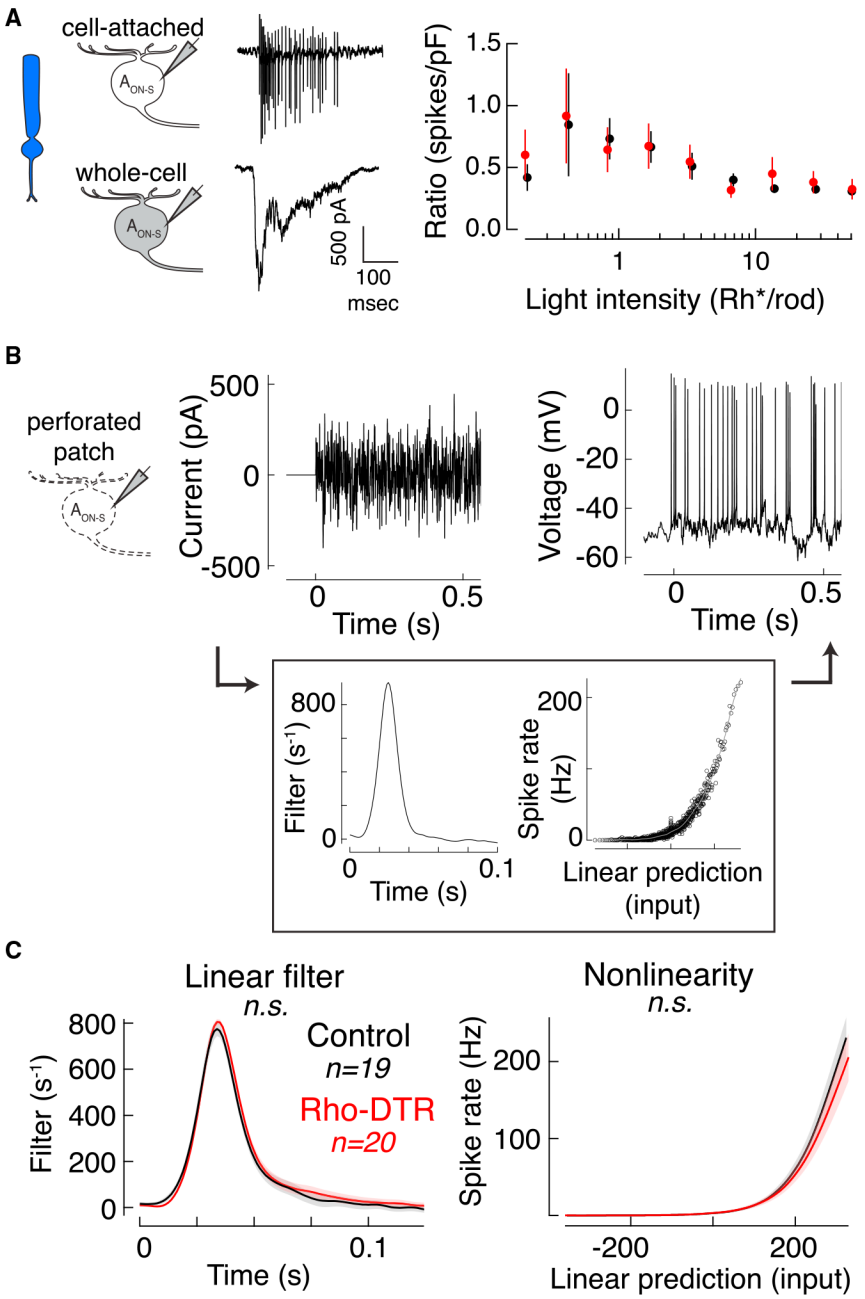

Figure 3. Intrinsic Excitability of A_{ON-S} Ganglion Cells Is Maintained at Rod Light Levels after Rod Loss

(A) Cartoons and example traces of the recordings used (left) in the calculation of the ratio of rod-mediated spike count to charge for each A_{ON-S} ganglion cell in which both measurements were made sequentially in the same cell (right). Points are mean ± SEM.

(B) Test of intrinsic excitability. Example of current injected through the patch pipette (left) and the resulting spikes (right) recorded in perforated patch configuration. Background was kept dark during the duration of the current injections, which were 40-s epochs for six or more repeats. (Box) Time-reversed spike-triggered average (left in box) and the nonlinearity for the example cell (right in box). Nonlinearity fit with a sigmoid function (gray).

(C) Time-reversed spike-triggered average (left) and average nonlinearity (right) of the linear-nonlinear model calculated from spike responses to white noise current injections (mean ± SEM). For the nonlinearity, abscissa represents the convolution between the spike-triggered average and the stimulus in units of standard deviation, i.e., linear prediction or generator potential. Ordinate represents the spike rate. The nonlinearity for each cell was interpolated and smoothed with a spline function. Permutation test shows that neither the linear filter nor nonlinearity are significantly different between control and Rho-DTR conditions.

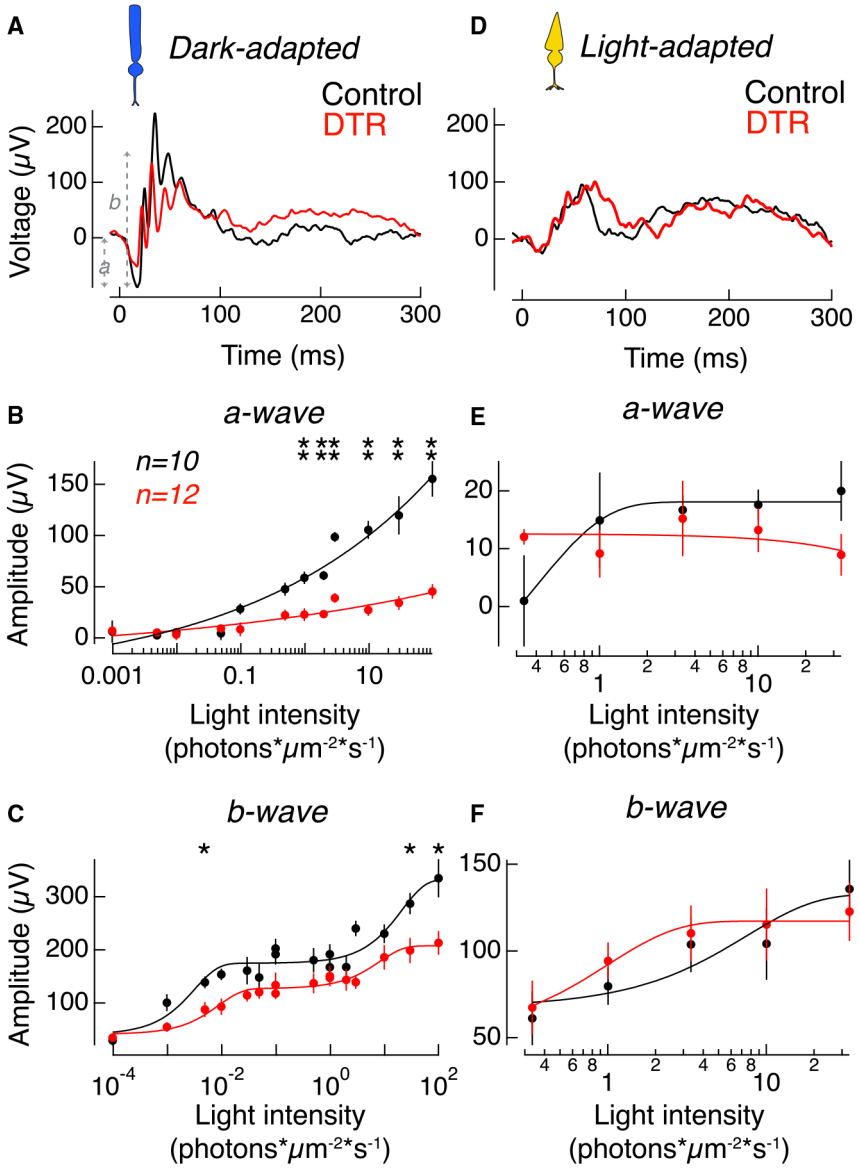

Figure 4. Rod-Mediated Responses Compromised but Postsynaptic and Cone-Mediated Responses Preserved in the Electroretinogram

(A) Example *in vivo* electroretinogram of control (black) and Rho-DTR (red) mice taken in the dark-adapted, rod-mediated condition at 2.919 photons*μm^{-2}*s^{-1}. Amplitude of a-wave was measured from baseline to the trough of the first negative peak. Amplitude of b-wave was measured from the trough of the first negative peak to the second-highest positive peak. (B) Average amplitude of the dark-adapted a-wave, which is the rod-mediated voltage response in the waveform, as a function of light intensity. Points are mean ± SEM. Significant differences between response amplitudes at each light intensity are denoted by asterisks above each pair of points (t test). Light intensities (p value); 0.973 photons*μm^{-2}*s^{-1} (0.030); 1.946 (0.0173); 2.919 (0.0043); 9.73 (0.0043); 29.19 (0.0087); and 97.3 (0.0043). (C) Average amplitude of the dark-adapted b-wave, which is the rod bipolar cell-mediated voltage response in the waveform, as a function of light intensity. Points are mean ± SEM.

Light intensity (p value); 0.04865 photons*μm^{-2}*s^{-1} (0.030); 29.29 (0.017); and 97.3 (0.030).

(D) Example *in vivo* electroretinogram of control (black) and Rho-DTR (red) mice taken in the light-adapted, cone-mediated condition.

(E) Average amplitude of the light-adapted a-wave, which is the cone-mediated voltage response in the waveform, as a function of light intensity. Points are mean ± SEM. No significant differences across light intensities (t test).

(F) Average amplitude of the light-adapted b-wave, which is the ON cone bipolar cell-mediated voltage response in the waveform, as a function of light intensity. Points are mean ± SEM. No significant differences across light intensities (t test). Electroretinograms taken 1 month after DT injection. Electroretinograms taken 3 days and ≥4 months after DT injection shown in Figure S6.

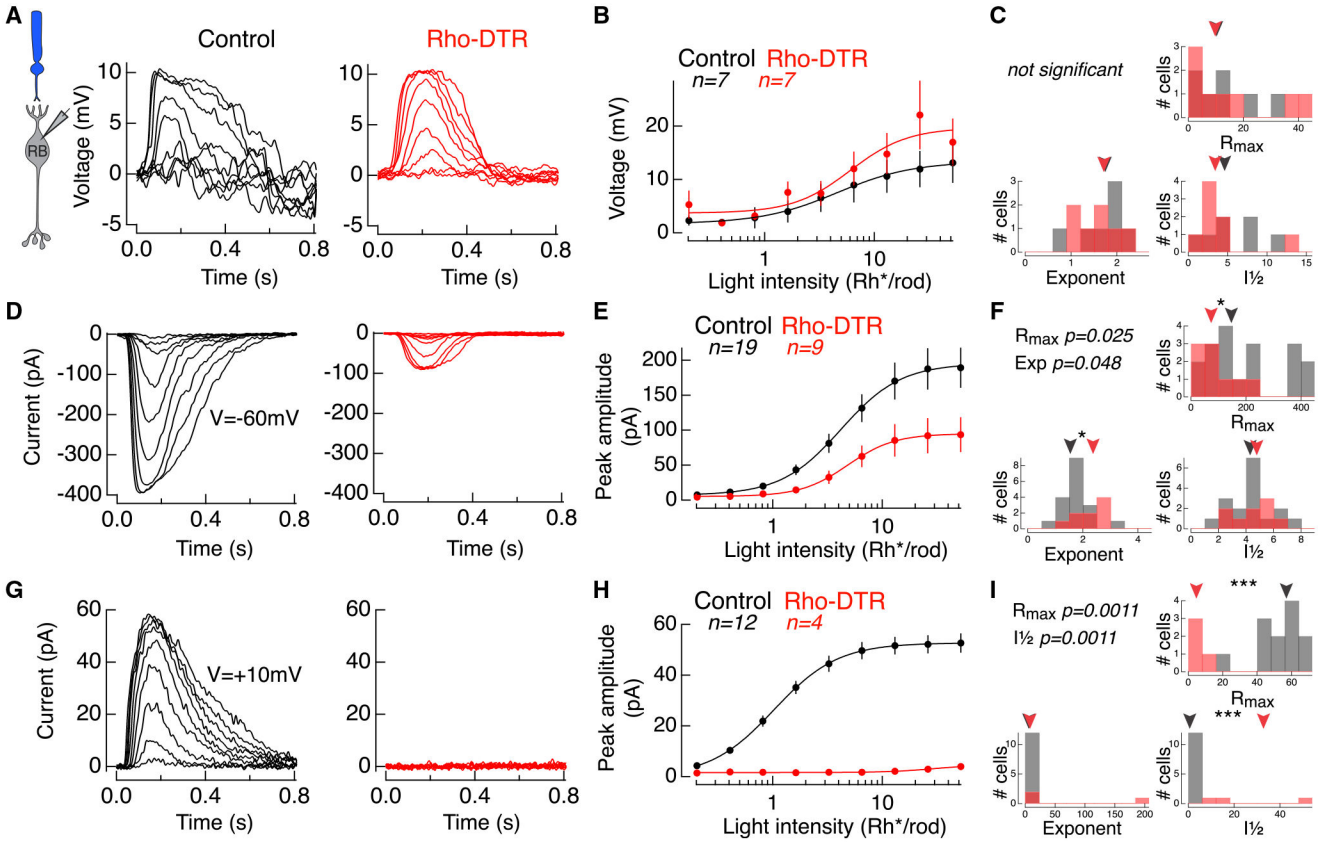

Figure 5. Compensated Voltage Responses in Rod Bipolar Cells Explained by Diminished Excitatory and Inhibitory Inputs

(A) Example rod-mediated voltage responses to a family of flashes in rod bipolar cells under current clamp in control (black) and Rho-DTR (red) conditions.

(B) Average intensity-response relationship for peak voltage response at each light intensity across rod bipolar cells. Points are mean ± SEM. Data fit with a Hill equation.

(C) Histogram of three fit parameters for the population of rod bipolar cell voltages in control and Rho-DTR conditions. (C, F, and I) Triangles above represent the median of each distribution, and asterisks denote significant differences between control and Rho-DTR populations by the rank sum test. Significant p values are reported in the upper left corner.

(D) Example rod-mediated excitatory current responses to a family of flashes in rod bipolar cells under voltage-clamp (V = −60 mV) in control (black) and Rho-DTR (red) conditions.

(E) Average intensity-response relationship for peak excitatory current responses at each light intensity across rod bipolar cells. Points are mean ± SEM. Data fit with a Hill equation.

(F) Histogram of fit parameters for the population of rod bipolar cell excitatory inputs in control and Rho-DTR conditions.

(G) Example rod-mediated inhibitory current responses to a family of flashes in rod bipolar cells under voltage clamp (V = +10 mV) in control (black) and Rho-DTR (red) conditions.

(H) Average intensity-response relationship for peak inhibitory current responses at each light intensity across rod bipolar cells. Points are mean ± SEM. Data fit with a Hill equation.

(I) Histogram of fit parameters for the population of rod bipolar cell inhibitory inputs in control and Rho-DTR conditions.

See also Figures S4 and S5 and Table S4.

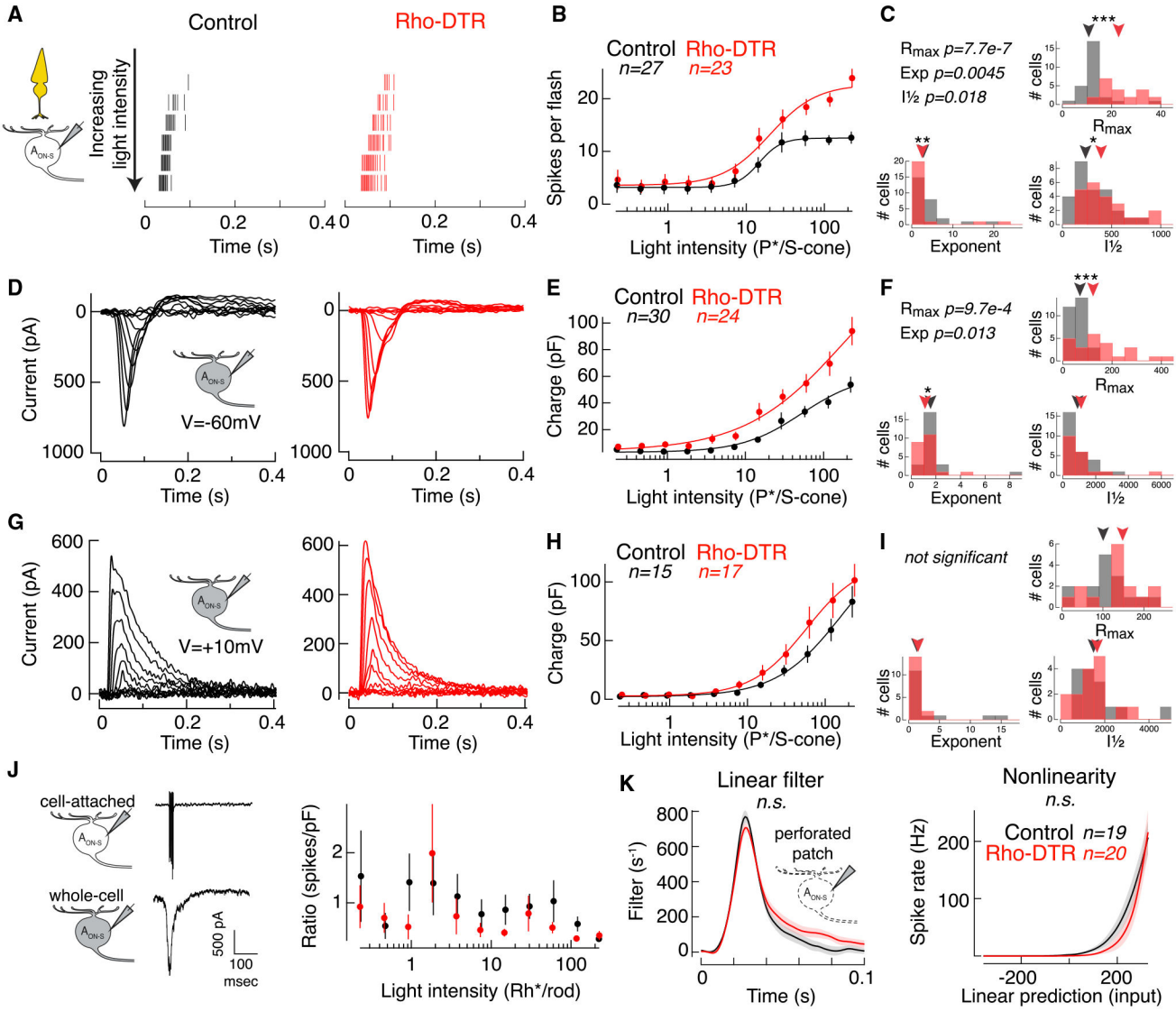

Figure 6. Cone-Mediated Spiking and Input Currents in A_{ON-S} Ganglion Cells Increase after Rod Loss

(A) Spike rasters from cell-attached recordings of A_{ON-S} ganglion cells in response to a cone-preferring stimulus: 10-ms flash at time 0 with the 370-nm LED on a mean of 4,000 Rh*/rod/s produced by the 470-nm LED to adapt rods. Each row shows the response to a flash doubling in intensity from top to bottom in control (black) and Rho-DTR (red) conditions.

(B) Average intensity-response relationship for the total number of spikes in response to each flash intensity. Points are mean ± SEM. (B, E, and H) Data points for each cell fit with a Hill equation, which can be captured by a maximum response (R_{max}), intensity at half maximum response (I½), and exponent.

(C) Histogram of fit parameters for the population of A_{ON-S} ganglion cells in control and Rho-DTR conditions. (C, F, and I) Triangles above represent the median of each distribution, and asterisks denote significant differences between control and Rho-DTR populations by the rank sum test. Significant p values are reported in the upper left corner.

(D) Excitatory currents from voltage-clamp recordings of $A_{ON\text{-}S}$ ganglion cells (V = −60 mV) in response to the same cone-mediated stimulus described above.
(E) Intensity-response relationship for the integral of the excitatory current.
(F) Histogram of Hill equation fits to the excitatory charge for individual cells.
(G) Inhibitory currents from voltage-clamp recordings of $A_{ON\text{-}S}$ ganglion cells (V = +10 to +60 mV, determined by reversal of the light response) in response to the same cone-mediated stimulus described above.
(H) Intensity-response relationship for the integral of the inhibitory current.
(I) Histogram of Hill equation fits to the inhibitory charge for individual cells.
(J) Cartoons and example traces of the recordings used (left) in the calculation of the ratio of cone-mediated spike count to charge calculated for each $A_{ON\text{-}S}$ ganglion cell in which both measurements were made in the same cell (right). Points are mean ± SEM.
(K) Time-reversed spike-triggered average (left) and average nonlinearity (right) of the linear-nonlinear model calculated from spike responses to white noise current injections (mean ± SEM) in perforated patch configuration. Blue mean of 4,000 Rh*/rod/s was applied to adapt rods for the duration of the current injections. For the nonlinearity, abscissa represents the convolution between the spike-triggered average and the stimulus in units of standard deviation, i.e., linear prediction or generator potential. Ordinate represents the spike rate. The nonlinearity for each cell was interpolated and smoothed with a spline function. Permutation test shows that neither the linear filter nor nonlinearity are significantly different between control and Rho-DTR conditions.
See also Table S5.

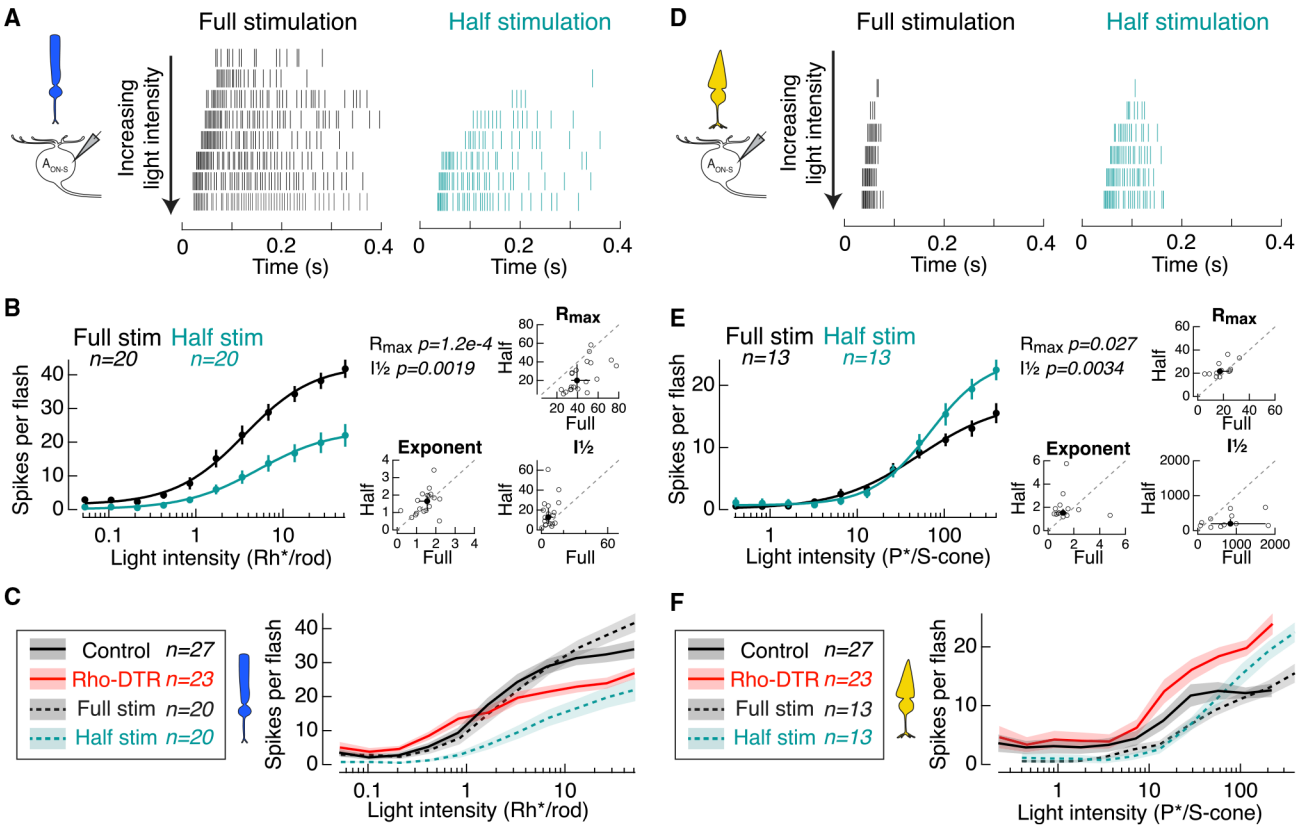

Figure 7. Half Stimulation of Control Retina Replicates Cone-but Not Rod-Mediated Responses in Rho-DTR Retina

(A) Spike rasters from cell-attached recordings of $A_{ON\text{-}S}$ ganglion cells in response to the rod-preferring stimulus. Each row shows the response to a flash doubling in intensity from top to bottom in full-stimulation (black) and half-stimulation (teal) conditions.

(B) Left: average intensity-response relationship for the total number of spikes in response to each flash intensity. Points are mean ± SEM. (B and E) Data points for each cell fit with a Hill equation, which can be captured by a maximum response (R_{max}), intensity at half maximum response (I½), and exponent. Right: fit parameters for which responses to both full and half stimulation were recorded in the same cell. Individual cells (open circles) and median ± IQR (closed circles with error bars). Dotted line indicates the line of slope unity. Significant p values by the Wilcoxon sign rank test reported in the upper left corner.

(C) Comparison of rod-mediated spike response from $A_{ON\text{-}S}$ ganglion cells from control retina (Control), control retina with full stimulation (Full stim), control retina with half stimulation (Half stim), and Rho-DTR retina indicates that Rho-DTR responses are partially recovered with respect to cells receiving half stimulation. “Control” and “Full stim” are both control retinas stimulated with full stimuli but acquired as separate control datasets. Lines and shaded regions are mean ± SEM.

(D) Spike rasters from cell-attached recordings of $A_{ON\text{-}S}$ ganglion cells in response to the cone-preferring stimulus. Each row shows the response to a flash doubling in intensity from top to bottom in full-stimulation (black) and half-stimulation (teal) conditions.

(E) Left: average intensity-response relationship for the total number of spikes in response to each flash. Right: fit parameters for which responses to both full and half stimulation were recorded in the same cell.

(F) Comparison of cone-mediated spike response from $A_{ON\text{-}S}$ ganglion cells as described in (C).

See also Table S6.

KEY RESOURCES TABLE

REAGENT or RESOURCE	SOURCE	IDENTIFIER
Antibodies		
Rabbit anti-Lucifer Yellow	Life Technologies	Cat# A5750; RRID:AB_1501344
Rabbit polyclonal anti-calbindin	Swant	Cat# CB38; RRID: AB_2721225
Mouse monoclonal anti-calbindin	Sigma	Cat# C9848; RRID:AB_476894
Goat anti-ChAT	Millipore	Cat# AB144P; RRID: AB_2079751
Rabbit polyclonal anti-cone arrestin	Millipore	Cat# AB15282; RRID:AB_1163387
Mouse monoclonal anti-CtBP2	BD Bioscience	Cat# 612044; RRID:AB_399431
Mouse monoclonal anti-Gephyrin	Synaptic Systems	Cat# 147 111; AB_2619837
Rabbit polyclonal anti-Iba1	Wako	Cat# 019-19741; RRID: AB_839504
Lectin peanut agglutinin, Alexa Fluor 647 Conjugate	Life Technologies	Cat# L32460
Mouse monoclonal anti-PKCalpha	Sigma-Aldrich	Cat# P5704; RRID:AB_477375
Rabbit anti-RBPMS	Phosphosolutions	Cat# 1830; RRID: AB_2492225
Rabbit polyclonal anti-Ribeye	Synaptic Systems	Cat# 192 103; RRID: AB_2086775
Mouse monoclonal anti-SMI-32	Stenberger Monoclonals	Cat# SMI-32P; RRID: AB_2314912
Donkey polyclonal anti-rabbit-Alexa 488	Jackson Immunoresearch	Cat# 711-545-152; RRID:AB_2313584
Donkey polyclonal anti-sheep-Alexa 633	Molecular Probes	Cat# A21100; RRID:AB_10374307
Donkey polyclonal anti-mouse-Dylight 405	Jackson Immunoresearch	Cat# 715-475-150; RRID:AB_2340839
Donkey polyclonal anti-mouse-Alexa 647	Jackson Immunoresearch	Cat# 715-605-151; RRID:AB_2340863
Chemicals, Peptides, and Recombinant Proteins		
Normal Donkey Serum	Jackson Immunoresearch	Cat# NC9624464
Ames' Medium	United States Biological	Cat# A1372-25
Agarose, low gelling temperature Type VIIA	Sigma Aldrich	Cat# A0701
Vectashield	Vector Laboratories	Cat# H-1000; RRID: AB_2336789
Amphotericin-B	Sigma Aldrich	Cat# A9528
Experimental Models: Organisms/Strains		
Mouse model: *C57BL/6-Gt(ROSA) 26Sortm1(HBEGF)Awai/J (DTR)*	The Jackson Laboratory	Cat# JAX:007900; RRID:IMSR_JAX:007900
Mouse model: *B6;SJL-Pde6b+ Tg(Rho-icre)1Ck/Boc (Rho-iCre)*	The Jackson Laboratory (Li et al., 2005)	Cat# JAX:015850 RRID: IMSR_JAX:015850
Mouse model: *B6.Cg-Gt(ROSA) 26Sortm6(CAG-ZsGreen1)Hze/J (Ai6)*	The Jackson Laboratory	Cat# JAX:007906; RRID:IMSR_JAX:007906
Mouse model: *Grm6-tdTomato*	Kerschensteiner et al., 2009	N/A
Software and Algorithms		
ImageJ	NIH	https://imagej.nih.gov/ij/, RRID: SCR_003070
Amira	Thermo-Fisher Scientific	https://www.thermofisher.com/global/en/home/industrial/electron-microscopy/electron-microscopy-instruments-workflow-solutions/3d-visualization-analysis-software.html, RRID: SCR_014305
Imaris	Bitplane	https://imaris.oxinst.com, RRID: SCR_007370
MATLAB	Mathworks	https://www.mathworks.com/products/matlab.htm, RRID: SCR_001622
Igor Pro	Igor Pro	RRID:SCR_000325

REAGENT or RESOURCE	SOURCE	IDENTIFIER
Object Finder	Della Santina et al., 2013	https://lucadellasantina.github.io/ObjectFinder/
Symphony and Stage	Mark Cafaro and Fred Rieke	https://github.com/Symphony-DAS/symphony-v1/wiki; https://github.com/Stage-VSS/stage-v1